N89-15937

1.0 INTRODUCTION

The Upper Atmosphere Research Satellite (UARS) has two definitive attitude determination requirements: the definitive attitude of the Modular Attitude Control Subsystem (MACS) and the definitive attitude of the gimbaled Solar-Stellar Pointing Platform (SSPP). The onboard computer (OBC) will compute the MACS attitude using a Kalman filter and will transform this attitude solution through the SSPP gimbals to calculate the SSPP attitude. The attitude ground support system (AGSS) will compute the MACS attitude using a batch least-squares differential corrector algorithm and will also transform this solution through the gimbals to obtain the SSPP attitude. This paper reports the results of a prelaunch study to predict the accuracy of the OBC attitude solutions and the accuracy of the AGSS attitude solutions. The OBC and AGSS solution accuracies are then compared to establish the relative quality.

The software that was used for both the OBC and the AGSS study is the Attitude Determination Error Analysis System (ADEAS) Program, Release 3 (CSC, 1986; Fang, 1983). ADEAS has the ability to estimate the accuracies of both a Kalman filter and a batch differential corrector. The ADEAS program has not at this time completed formal acceptance testing; therefore, while the results presented here are considered essentially correct, they may be updated in the future.

The attitude sensors that can be used by the OBC or the AGSS are two fixed-head star trackers (FHSTs), the inertial reference unit (IRU), and the fine Sun sensor (FSS) on the MACS. Normally, two FHSTs will be used for attitude determination and control. In the event that one FHST fails, the FSS on the MACS is to be used in conjunction with the remaining FHST. In this study, the attitude uncertainty has been estimated for the case of two FHSTs. The IRU drift rate bias uncertainties are always solved in addition to the attitude uncertainties.

The stars used in this analysis are taken from the combined OBC primary and secondary catalogs as presented in Sheldon (1986). Every estimate of the attitude uncertainty was repeated for two cases of star observability: (1) When the spacecraft is flying in an orbit such that each FHST can see the maximum number of stars (29 stars) with minimum star separation angles, this

represents the best-case star observability during the UARS mission. (2) When the spacecraft is flying in an orbit such that each FHST can see the minimum number of stars (5 stars) with maximum star separation angles, this represents the worst-case star observability during the UARS mission. These two cases will be referred to as the 29-star case and the 5-star case, respectively. The timespan for all cases is one full orbit, 5796 seconds (sec). The resulting attitude uncertainties presented are those at the end of the data batch.

The UARS ephemeris is generated internally in ADEAS with no orbit perturbations and no atmospheric drag. For the 29-star case, the spacecraft is flying forward and the FHSTs are pitching about the axis of negative orbit normal, which is at a right ascension (RA) of 306 degrees (deg) and a declination (dec) of -33 deg. For the 5-star case, the spacecraft is flying backward and the two FHSTs are pitching about the axis of orbit normal, which is at RA of 118 deg and dec of 33 deg. The Keplerian orbital elements used in the study represent the nominal mission orbit:

Semimajor axis = 6.978065×10^6 meters

Eccentricity = 0.001486

Inclination = 57.017788 deg

Argument of perigee = 60.9378 deg

Mean anomaly = 299.162 deg

$$\text{Right ascension of ascending node} = \begin{cases} 216 \text{ deg for 29-star case} \\ 208 \text{ deg for 5-star case} \end{cases}$$

The epoch time is not important in the uncertainty analysis, as it is only used as a time reference in the calculation.

2.0 PRELAUNCH SENSOR PARAMETERS

This section reviews values of the sensor parameters that will be known at the time of launch, including the prelaunch estimates for sensor noise and alignment uncertainties and the nominal alignments of the sensors. The nominal orientations of the attitude sensors on the spacecraft are represented by Euler angle rotations from the MACS frame.

2.1 FHST

The nominal orientations of the FHSTs are given as a 2-1-3 Euler sequence. The Euler angles and the nominal fields of view (FOVs) are given in Table 1.

Table 1. Nominal FHST Alignments and FOV Sizes

Sensor	Rotation Angles (Degrees)			FOV (Degrees)
	θ_1	θ_2	θ_3	
FHST A	-114.27	-49.27	0	8 x 8
FHST B	114.27	-49.27	0	8 x 8

The prelaunch value of the FHST noise is derived from the 3σ error budget for an 8-degree-diameter circular FOV as presented in GE (1983). The components of the total noise are given in Table 2. The values are given in both radians and arc-seconds (arc-sec).

Table 2. Prelaunch FHST Noise Sources (GE, 1983)

Noise Source	Value (3σ)	
	(Radians)	(Arc-Sec)
Noise Equivalent Angle	1.193×10^{-4}	24.6
Quantization Error	3.394×10^{-5}	7.0
Signal Lag Error (Unsynch)	3.636×10^{-5}	7.5
Calibration Error	1.454×10^{-4}	30.0

The noise equivalent angle and the signal lag error are assumed to be random white noise. The quantization error listed in Table 2 is actually the quantization interval. The standard deviation of the random error generated by a quantized process is $\sqrt{1/12}$ times the quantization interval (Bendat, 1971). The 3σ value, therefore, for the quantization error should be 2.939×10^{-5} radians (6.1 arc-sec). The root-sum-square (RSS) of these four noises is

1.939×10^{-4} radians (40.0 arc-sec). This number is adopted for the FHST noise.

The 3σ prelaunch FHST alignment uncertainties are provided by GE (1988): 2.681×10^{-4} radians (55.3 arc-sec) for both the X- and Y-axes and 2.676×10^{-4} radians (55.2 arc-sec) for the boresight direction, the Z-axis.

2.2 IRU

If a spacecraft is moving with constant angular velocity, the IRU misalignments and scale factors are indistinguishable from the drift rate biases. This condition is very closely met by UARS when it is in normal pointing mode. Because both the OBC and the AGSS solve for the IRU biases as well as the attitude, the contribution to the attitude uncertainty by the misalignment and scale factor uncertainties is automatically taken into account. The IRU noise does not contribute significantly to the attitude uncertainty and was, therefore, not considered in this study.

2.3 SSPP

The SSPP is mounted on a two-axis gimbal system. When both gimbals are in their nominal zero positions, the SSPP coordinate system aligns with the MACS frame. The α-gimbal is fixed to the spacecraft and rotates about the MACS Y-axis. It has a range of 0 to 360 degrees although, in actual use, the range is restricted by spacecraft and Earth blockage. The β-gimbal is carried by the α-gimbal and rotates about the SSPP X-axis. The β-gimbal has a range of 0 to 90 degrees; however, in normal Sun-tracking operation, β will not exceed 80 degrees. (This is the sum of the UARS orbital inclination and the maximum elevation of the Sun.) A more complete description of the SSPP geometry is presented in the UARS FDSS Mathematical Background (Kast, 1987b).

The relevant uncertainties with regard to the SSPP are the alignment uncertainty from the MACS to the SSPP gimbals, the uncertainties of the gimbal measurements, the alignment uncertainty from the gimbals to the SSPP FSS, and the noise of the SSPP FSS. The prelaunch estimates of each of these uncertainties are given below. All values are 3σ.

The uncertainties σ_α and σ_β in the two gimbal measurements have values of 9.696×10^{-5} radians (20.0 arc-sec) each (GE, 1986).

The SSPP FSS noise uncertainty is taken from Adcole (1986). The value of the uncertainty is $\sigma_{FSS} = 1.745 \times 10^{-4}$ radians (36.0 arc-sec).

The prelaunch alignment uncertainties are taken to be diagonal matrices of the form

$$P_{\alpha m} = \begin{bmatrix} \sigma^2_{\alpha m} & 0 & 0 \\ 0 & \sigma^2_{\alpha m} & 0 \\ 0 & 0 & \sigma^2_{\alpha m} \end{bmatrix} \qquad P_{N\beta} = \begin{bmatrix} \sigma^2_{N\beta} & 0 & 0 \\ 0 & \sigma^2_{N\beta} & 0 \\ 0 & 0 & \sigma^2_{N\beta} \end{bmatrix}$$

where $P_{\alpha m}$ and $P_{N\beta}$ are the covariance matrices of the MACS-to-gimbals and gimbals-to-SSPP-FSS alignments, respectively. The uncertainties $\sigma_{\alpha m}$ and $\sigma_{N\beta}$ were derived from data in Neste (1987). The values used are 6.545×10^{-4} and 2.424×10^{-4} radians (135 and 50.0 arc-sec), respectively.

3.0 FHST ON-ORBIT ALIGNMENT ACCURACY

The on-orbit alignment for the two FHSTs will be performed shortly after launch. The algorithm presented in Shuster (1982) is used by the UARS AGSS. This scheme minimizes the overall deviation of the sensor alignments from their prelaunch values. The covariances of the misalignments after on-orbit alignment for two sensors can be estimated by

$$P(post)^{-1} = \left[\begin{array}{c|c} G & -G \\ \hline -G & G \end{array}\right] + \left[\begin{array}{c|c} P_1(pre)^{-1} & 0 \\ \hline 0 & P_2(pre)^{-1} \end{array}\right]$$

where

$P(post)$ = 6 by 6 postcalibration misalignment covariance matrix

$$G = \sum_{m=1}^{N} \frac{\left[\hat{W}_1^m \times \hat{W}_2^m\right]\left[\hat{W}_1^m \times \hat{W}_2^m\right]^T}{\left[\sigma_1^2 + \sigma_2^2\right]\left|\hat{W}_1^m \times \hat{W}_2^m\right|^2}$$

N = number of observations

σ_i^2 = sensor noise for sensor i

$\hat{W}_i^m$ = m^{th} star vector observation tracked by sensor i, expressed in spacecraft body coordinates

$P_{i(pre)}$ = 3 by 3 precalibration misalignment covariance matrix for sensor i

Because this alignment algorithm is attitude independent, it requires that the star observations in the two sensors be simultaneous. Based on this algorithm, a small program simulating the two FHSTs on UARS was developed to estimate the uncertainties of the misalignments after on-orbit alignment.

In estimating the uncertainties, it is assumed that UARS will be deployed on October 26, 1991 (an arbitrary date in late October 1991). To maximize the period before the first yaw maneuver, it is also assumed that the spacecraft is flying backward in an orbit whose right ascension of the ascending node is equal to the right ascension of the Sun. The two FHSTs are assumed to be aligned shortly after deployment using two orbits of FHST data with a total of 21 simultaneous star observations. The resultant alignment uncertainties are given in Table 3.

Table 3. FHST On-Orbit Alignment Uncertainties

Sensor	Axis	Alignment Uncertainty (3σ)	
		(Radians)	(Arc-Sec)
FHST A	X	2.123×10^{-4}	43.8
	Y	2.468×10^{-4}	50.9
	Z	2.642×10^{-4}	54.5
FHST B	X	2.123×10^{-4}	43.8
	Y	2.482×10^{-4}	51.2
	Z	2.633×10^{-4}	54.3

Further simulation runs indicate that these accuracies are not significantly improved by using more data.

4.0 UARS ATTITUDE DETERMINATION ACCURACY USING A KALMAN FILTER

The UARS OBC attitude determination algorithm is a Kalman filter. This filter propagates the previous attitude solution using IRU data whenever there are no valid star observations. When there is a valid star observation, the OBC

updates its estimate of the state vector, which consists of the IRU drift rate bias and the attitude. This update occurs at intervals of 32.768 seconds. When there are valid star observations in both FHSTs, the OBC updates the state vector using data from the FHST that was used longest ago. This situation produces an effective FHST sampling rate of 65.536 seconds with the observations being taken alternately for the two sensors.

The error estimation software used in this study cannot model an alternating sampling of the FHSTs. To estimate the effect of the alternating sampling, the program was run for both a 32.768-second and a 65.536-second sampling rate. The resulting variances were averaged together with a weighting proportional to the fraction of time that observations overlapped, that is, the fraction of time when there were valid observations in both FHSTs. In the 5-star case, there is no overlap; in the 29-star case, there is approximately a 65 percent overlap.

In the 5-star case, the attitude uncertainties were taken at the end of a three-orbit run because the Kalman filter had not converged at the end of the first orbit.

4.1 RESULTS USING PRELAUNCH PARAMETERS

The OBC attitude solution uncertainties using the prelaunch values of the attitude sensor uncertainties presented in Section 2.0 are given below. For the two cases of star observability, as discussed in the introduction, the attitude uncertainties are given in Table 4.

Table 4. OBC Attitude Uncertainties Using Prelaunch Alignment Uncertainties

Case	Axis	Attitude Uncertainty (3σ)	
		(Radians)	(Arc-Sec)
5-star	X	1.572×10^{-4}	32.4
	Y	3.132×10^{-4}	64.6
	Z	1.584×10^{-4}	32.7
29-star	X	1.352×10^{-4}	27.9
	Y	3.092×10^{-4}	63.8
	Z	1.321×10^{-4}	27.2

4.2 RESULTS USING ON-ORBIT ALIGNMENT ESTIMATES

The AGSS attitude solution uncertainties using the on-orbit estimates of the FHST alignment uncertainties presented in Section 3.0 are given in Table 5.

Table 5. OBC Attitude Uncertainties Using On-Orbit FHST Alignment Uncertainties

Case	Axis	Attitude Uncertainty (3σ)	
		(Radians)	(Arc-Sec)
5-star	X	1.406×10^{-4}	29.0
	Y	2.875×10^{-4}	59.3
	Z	1.262×10^{-4}	26.0
29-star	X	1.195×10^{-4}	24.7
	Y	2.830×10^{-4}	58.4
	Z	1.036×10^{-4}	21.4

5.0 UARS ATTITUDE DETERMINATION ACCURACY USING A DIFFERENTIAL CORRECTOR

The AGSS definitive attitude determination system is a batch least-squares differential corrector that estimates an epoch attitude and drift rate biases of the IRU over a batch of approximately one orbit of sensor data. This epoch attitude is propagated to uniform time intervals using the IRU data and the

solved IRU biases. The results given in this section are the attitude covariances at the end of a one-orbit batch of data. It is assumed that data from both FHSTs are available every 32.768 seconds when there are valid stars in the FOV.

5.1 RESULTS USING PRELAUNCH PARAMETERS

The AGSS attitude solution uncertainties using the prelaunch values of the attitude sensor uncertainties presented in Section 2.0 are given below. For the two cases of star observability, as discussed in the introduction, the attitude uncertainties are given in Table 6.

Table 6. AGSS Attitude Uncertainties Using Prelaunch Alignment Uncertainties

Case	Axis	Attitude Uncertainty (3σ)	
		(Radians)	(Arc-Sec)
5-star	X	1.733×10^{-4}	35.7
	Y	3.143×10^{-4}	64.8
	Z	0.800×10^{-4}	16.5
29-star	X	1.582×10^{-4}	32.6
	Y	3.009×10^{-4}	62.1
	Z	1.452×10^{-4}	29.9

5.2 RESULTS USING ON-ORBIT ALIGNMENT ESTIMATES

The AGSS attitude solution uncertainties using the on-orbit estimates of the FHST alignment uncertainties presented in Section 3.0 are given in Table 7.

Table 7. AGSS Attitude Uncertainties Using On-Orbit FHST Alignment Uncertainties

Case	Axis	Attitude Uncertainty (3σ)	
		(Radians)	(Arc-Sec)
5-star	X	1.395×10^{-4}	28.8
	Y	2.900×10^{-4}	59.8
	Z	0.679×10^{-4}	14.0
29-star	X	1.384×10^{-4}	28.5
	Y	2.763×10^{-4}	57.0
	Z	1.156×10^{-4}	23.8

6.0 SSPP ATTITUDE DETERMINATION ACCURACY

This section reports estimates of the SSPP on-orbit misalignment determination accuracy and the SSPP attitude accuracies using both the estimated OBC attitude solution accuracy and the estimated AGSS attitude solution accuracy.

The SSPP attitude is represented as a transformation from the geocentric inertial (GCI) coordinate system to the SSPP coordinate system. This transformation can be expressed as a series of rotations

$$M_{NI} = M_{N\beta}\, M_{\beta\alpha}\, M_{\alpha m}\, M_{mI}$$

where M_{NI} is the SSPP attitude matrix, $M_{N\beta}$ and $M_{\alpha m}$ represent misalignments of the β-gimbal and the α-gimbal, respectively, $M_{\beta\alpha}$ is the product of two Euler rotation matrices about the two gimbal axes:

$$M_{\beta\alpha} = M_1(\beta)\, M_2(\alpha)$$

and M_{mI} represents the MACS attitude. The total SSPP attitude covariance matrix, P_{NI}, may be calculated from the transformations in the above equations and their corresponding covariance matrices as follows (Kast, 1987a, Section 3.1.1.7):

$$P_{NI} = M_{N\beta}\left[M_{\beta\alpha}(M_{\alpha m}P_{mI}M_{\alpha m}^T + P_{\alpha m})M_{\beta\alpha}^T + P_{\beta\alpha}\right]M_{N\beta}^T + P_{N\beta}$$

P_{mI} is the attitude covariance of either the OBC or the ground AGSS attitude solution, $P_{\alpha m}$ and $P_{N\beta}$ are the covariance matrices for the SSPP misalignment matrices, and $P_{\beta\alpha}$ is the covariance of the gimbal rotation. $P_{\beta\alpha}$ is computed from the prelaunch values for the gimbal rotation uncertainties and depends on the measured α and β angles:

$$P_{\beta\alpha} = \begin{bmatrix} \sigma_\beta^2 & 0 & 0 \\ 0 & \sigma_\alpha^2 \cos^2\beta & -\sigma_\alpha^2 \cos\beta \sin\beta \\ 0 & -\sigma_\alpha^2 \cos\beta \sin\beta & \sigma_\alpha^2 \sin^2\beta \end{bmatrix}$$

6.1 SSPP ON-ORBIT ALIGNMENT ESTIMATION RESULTS

In solving for the on-orbit estimate of the SSPP misalignment, the misalignment matrices are assumed to be small angle rotations of the form

$$M_{\alpha m} = \begin{bmatrix} 1 & \varepsilon_3 & -\varepsilon_2 \\ -\varepsilon_3 & 1 & \varepsilon_1 \\ \varepsilon_2 & -\varepsilon_1 & 1 \end{bmatrix}, \qquad M_{N\beta} = \begin{bmatrix} 1 & \delta_3 & -\delta_2 \\ -\delta_3 & 1 & \delta_1 \\ \delta_2 & -\delta_1 & 1 \end{bmatrix}$$

The angles ε_1, ε_2, ε_3 represent small rotations about the MACS axes, and the angles δ_1, δ_2, δ_3 represent small rotations about the SSPP axes. The angles ε_2 and δ_1 are equivalent to α- and β-gimbal angle biases, respectively.

A FORTRAN program was written to estimate the misalignment covariance matrices, $P_{\alpha m}$ and $P_{N\beta}$. Following Section 13.4 of Spacecraft Attitude Determination and Control (Wertz, 1984), a single 6-by-6 covariance matrix containing $P_{\alpha m}$ and $P_{N\beta}$ in the upper left and lower right, respectively, is computed assuming that the misalignment matrices were computed using a batch least squares differential corrector having the state vector (ε_1, ε_2, ε_3, δ_1, δ_2, δ_3).

To compute the misalignment covariances, it is necessary to assume a MACS attitude covariance for use in constructing an observation weight matrix. Because the SSPP misalignments will be calculated on the ground, the covariance used was the differential corrector results after on-orbit alignment of the FHSTs for the 29-star case as described in Section 5.0. Estimates of the accuracies of only the angles ε_1, ε_2, ε_3, and δ_1 are made as the remaining two angles were found to have poor observability. The resulting SSPP misalignment covariance matrices (in radians^2) are as follows:

$$P_{\alpha m} = \begin{bmatrix} 3.317 \times 10^{-11} & -1.337 \times 10^{-11} & -0.353 \times 10^{-11} \\ -1.337 \times 10^{-11} & 3.003 \times 10^{-11} & 1.494 \times 10^{-11} \\ -0.353 \times 10^{-11} & 1.494 \times 10^{-11} & 3.369 \times 10^{-11} \end{bmatrix}$$

and

$$P_{N\beta} = \begin{bmatrix} 3.839 \times 10^{-11} & 0 & 0 \\ 0 & 6.529 \times 10^{-9} & 0 \\ 0 & 0 & 6.529 \times 10^{-9} \end{bmatrix}$$

More information concerning the SSPP misalignment accuracy estimation is provided by Bosl (1987).

6.2 SSPP ATTITUDE ACCURACY USING KALMAN FILTER RESULTS

Table 8 presents the SSPP attitude uncertainties using the MACS attitude covariance of the OBC solution and the equations presented in Section 6.1. The values reported are after on-orbit alignment of the FHSTs. Because the SSPP attitude uncertainty for each SSPP axis depends on the gimbal angles, a typical gimbal position of α equal to 180 degrees and β equal to 45 degrees was chosen for reporting the per-axis uncertainty. The RSS of the three axes is independent of the gimbal angles and is also reported in Table 8.

Table 8. SSPP Attitude Uncertainties Using OBC Attitude Uncertainties After On-Orbit FHST Alignment

Case	Axis	Attitude Uncertainty (3σ)	
		(Radians)	(Arc-Sec)
5-star	X	1.726×10^{-4}	35.6
	Y	3.434×10^{-4}	70.8
	Z	3.289×10^{-4}	67.8
	RSS	5.059×10^{-4}	104.3
29-star	X	1.560×10^{-4}	32.2
	Y	3.374×10^{-4}	69.6
	Z	3.232×10^{-4}	66.7
	RSS	4.926×10^{-4}	101.6

6.3 SSPP ATTITUDE ACCURACY USING DIFFERENTIAL CORRECTOR RESULTS

The SSPP attitude uncertainties resulting from the AGSS attitude solution covariance after on-orbit FHST alignment are given in Table 9. As in Section 6.2, these values are at gimbal angles of α equal to 180 degrees and β equal to 45 degrees.

Table 9. SSPP Attitude Uncertainties Using AGSS Attitude Uncertainties After On-Orbit FHST Alignment

Case	Axis	Attitude Uncertainty (3σ)	
		(Radians)	(Arc-Sec)
5-star	X	1.718×10^{-4}	35.4
	Y	3.293×10^{-4}	67.9
	Z	3.283×10^{-4}	67.7
	RSS	4.957×10^{-4}	102.2
29-star	X	1.708×10^{-4}	35.2
	Y	3.387×10^{-4}	69.9
	Z	3.201×10^{-4}	66.0
	RSS	4.963×10^{-4}	102.4

7.0 CONCLUSIONS

Comparison of the estimates of the OBC and AGSS attitude determination uncertainties shows no significant differences. The ADEAS results indicate that most of the uncertainty for both the OBC and the AGSS is due to the effect of the FHST alignment uncertainties. This effect is the reason that there is little difference between the 5-star case and the 29-star case. The FHST alignment uncertainties given in Table 3 are not much less than the prelaunch values. This result is due to attempting to estimate six uncertainty values when three of the six degrees of freedom are unobservable. There is, therefore, a strong, unavoidable dependence on the prelaunch alignment uncertainties.

For all cases, the X- and Z-axes have 3σ uncertainties of approximately 1.454×10^{-4} radians (30 arc-sec), and the Y-axis has a 3σ uncertainty of approximately 2.909×10^{-4} radians (60 arc-sec). Based on the results of this study, it is recommended that these uncertainties be used in UARS error budget analyses.

REFERENCES

Adcole Corporation, "Critical Design Review Data Package: Platform Sun Sensor," SVS 11064, November 19, 1986

Bendat, J. S. and A. G. Pierool, Random Data: Analysis and Measurement Procedures, New York: Wiley-Interscience, 1971

Bosl, W., "Solar-Stellar Pointing Platform (SSPP) Definitive Attitude Accuracy Study," Computer Sciences Corporation, CSC/TM-87/6020, Mission Report 87004, 1987

Computer Sciences Corporation, Attitude Determination Error Analysis System (ADEAS) User's Reference Manual, CSC/SD-86/6025, December 1986

Fang B. and W. Davis, Attitude Determination Error Analysis (ADEAS) Program Requirements and Mathematical Specifications, Computer Sciences Corporation, CSC/TM-83/6175, December 1983

General Electric, Instrument Module Attitude Determination Study for Upper Atmosphere Research Satellite, 83SDS4202, January 1983

General Electric, "SSPP Controls Presentation", June 13, 1986

General Electric, UARS Attitude Determination and Control Subsystem Level, Critical Design Review, February 2, 1988

Kast, J. K., K. Krack, et al., Upper Atmosphere Research Satellite (UARS) Flight Dynamics Support System (FDSS) Specifications Volume II: Functional Specifications, Computer Sciences Corporation, CSC/TR-86/6003, May 1987a

Kast, J. K., K. Krack, et al., Upper Atmosphere Research Satellite (UARS) Flight Dynamics Support System (FDSS) Mathematical Background, Computer Sciences Corporation, CSC/TM-86/6060, May 1987b

Neste, S. L., UARS Pointing Error Budgets, General Electric PIR U-1K21-UARS-517A, March 20, 1987

Sheldon, K., On-Board Star Catalog for UARS, General Electric PIR U-1k21-UARS-318, January 1986

Shuster, M.D, "In-Flight Estimation of Spacecraft Attitude Sensor Accuracies and Alignments," J Guidance, July-August 1982, vol. 5, vo. 4, pp. 339-343

Wertz, J. R. (ed.), Spacecraft Attitude Determination and Control, Dortrecht, Holland: D. Reidel Publishing Co., 1984

Maneuvering Strategies Using CMGs

H.S. Oh and S.R. Vadali
Department of Aerospace Engineering
Texas A&M University
College Station, TX 77843

ABSTRACT

This paper considers control strategies for maneuvering spacecraft using Single-Gimbal Control Momentum Gyros. A pyramid configuration using four gyros is utilized. Preferred initial gimbal angles for maximum utilization of CMG momentum are obtained for some known torque commands. Feedback control laws are derived from the stability point of view by using the Liapunov's Second Theorem. The gyro rates are obtained by the pseudo-inverse technique. The effect of gimbal rate bounds on controllability are studied for an example maneuver. Singularity avoidance is based on limiting the gyro rates depending on a singularity index.

INTRODUCTION

Control Moment Gyros (CMGs) are attractive spacecraft attitude control devices. They require no expendable propellant, which are of limited quantity and may contaminate the spacecraft environment. Their fixed rotor speeds minimize structure dynamic excitations. They are also capable of rapid slewing maneuvers and precision pointing. There are two types of CMGs; single-gimbal and double-gimbal.

The single-gimbal CMGs have the advantages of possessing relative mechanical simplicity and producing amplified torques directly on the spacecraft. However, development of control laws for their use is made difficult by the existence of internal singular states. External singular states correspond to directional angular momentum saturation. For any system of n CMGs and any direction in space, there exists a set of 2^n gimbal angles for which no torque can be produced in that direction [1]. For double-gimbal CMGs in parallel configuration, Kennel's law [2] has seen wide applications. In this paper, four single-gimbal CMGs in a pyramid configuration (as depicted in Fig. 1) are utilized.

Margulies and Aubrun [1] present a geometric theory of CMG systems. They characterize the momentum envelope of a cluster of CMGs and identify the internal singular states. Yoshikawa [3] presents a steering law for a roof-type configuration with four CMGs. His steering law is based on making all the internal singular states unstable by providing two jumps with hystereses around the singularities. Cornick [4] developed singularity avoidance control laws for the pyramid configuration. His technique is based on the ability to calculate the instantaneous locations of all singularities. Hefner and McKenzie [5] developed a technique for maximizing the minimum torque capability of a cluster of CMGs in the pyramid configuration. Recently Bauer

[6] showed that it is impossible to avoid some singularities and in general, no global singularity avoidance steering law can exist.

In the existing literature, the most commonly used steering law is based on the pseudo-inverse technique. Neglecting the effect of spacecraft rotation, the angular momentum H of the CMG cluster evolves as

$$\frac{d\underline{H}}{dt} = \underline{T} \tag{1}$$

where $\underline{T}$ is the torque demand.
This can also be written as

$$\frac{d\underline{H}}{dt} = C\dot{\underline{\sigma}} \tag{2}$$

where C is a matrix function of the gimbal angles $\underline{\sigma}$. From Eq. (1) and (2), we obtain

$$C\dot{\underline{\sigma}} = \underline{T} \tag{3}$$

Generally at least four CMGs are used for three-axis attitude control. Hence the pseudo-inverse is utilized to obtain gimbal rate commands from the torque command:

$$\dot{\underline{\sigma}} = C^T(CC^T)^{-1}\underline{T} \tag{4}$$

Some steering laws also employ null motion, i.e. gyro rate commands that produce no torque. Any null motion rate command $\dot{\underline{\sigma}}_N$ can be expressed as

$$\dot{\underline{\alpha}}_N = ([I] - C^T(CC^T)^{-1}C)\,\underline{V} \tag{5}$$

where $[I]$ is the identity matrix of the same dimension as the number of gyros and $\underline{V}$ is any arbitrary vector of appropriate dimension. The fact that $\dot{\underline{\alpha}}_N$ commands do not produce any torques can be verified by premultiplying C throughout Eq. (5).

The basis for singularity avoidance has been to provide appropriate null motion along with torque providing motion so that the required torques are produced as well as singular states are avoided. Typically, at singular states some of the gyros develop anti-parallel momentum configurations. Thereby their full momentum capability cannot be utilized.

In this paper we present results pertaining to the following aspects of torque generation using CMGs:

1) Investigation of the existence of preferred initial gimbal angles at zero momentum, for given torque commands such that the maximum momentum capability is utilized.

2) Feedback control of rotational maneuvers of spacecraft by using Liapunov's second theorem and investigation of the effects of gimbal rate bounds on controllability and performance.

SYSTEM EQUATIONS OF MOTION

An arbitrary asymmetric spacecraft, with the location of the ith single-gimbal gyro, is shown in Fig. 2. Spacecraft attitude is represented by Euler parameter vector $\underline{\beta}$. The differential equations for the attitude are given by the angular velocity vector $\bar{\omega}$ of the vehicle and an orthogonal attitude matrix $G(\beta)$ as follows:

$$\dot{\underline{\beta}} = \frac{1}{2} G(\beta)\, \bar{\omega} \tag{6}$$

where $\bar{\omega} = \begin{Bmatrix} 0 \\ \omega_x \\ \omega_y \\ \omega_z \end{Bmatrix}$ and $G(\beta) = \begin{bmatrix} \beta_0 & -\beta_1 & -\beta_2 & -\beta_3 \\ \beta_1 & \beta_0 & -\beta_3 & \beta_2 \\ \beta_2 & \beta_3 & \beta_0 & -\beta_1 \\ \beta_3 & -\beta_2 & \beta_1 & \beta_0 \end{bmatrix}$

To derive the equations of motion, we follow Junkins and Turner [7]. The detailed notation appears at the end of the paper. Ross and Melton [8] present an alternate formulation for double-gimbal CMG systems.

The total angular momentum of the system $\underline{H}^{s/c}$ about the system mass center c is composed of the vehicle's angular momentum and that of the CMGs as follows

$$\underline{H}^{s/c} = \underline{H}^{v/c} + \sum_{i=1}^{n} \underline{H}^{G_i/c} .$$

Each angular momentum can be expressed in vehicle frame $\{\hat{\underline{v}}\}$ as

$$\underline{H}^{v/c} = I^{v/c}\, \underline{\omega} , \quad \text{and}$$

$$\underline{H}^{G_i/c} = m_i (r_i \times \dot{\underline{r}}_i) + \underline{H}^{G_i/cG_i}$$

$$= M_i\, \underline{\omega} + \underline{H}^{G_i/cG_i} .$$

Then the system angular momentum can be written as

$$\underline{H}^{S/C} = (I^{V/C} + \Sigma M_i)\underline{\omega} + \Sigma \underline{H}^{G_i/cG_i}$$

$$= I\underline{\omega} + \Sigma \underline{H}^{G_i/cG_i}$$

where $I = I^{V/C} + \Sigma M_i$, i.e. the inertia matrix of vehicle body and point-massed gyro cluster about the c in vehicle frame.

For the convenience of simulation, we assume that

1) the center of the pyramid bottom surface coincides with the mass center c of the system.

2) the principal axes coincide with the axes of the vehicle frame $\{\hat{\underline{v}}\}$.

3) Only the relative axial angular momenta of the gyros are retained.

With these assumptions, the system angular momentum in vehicle frame can be expressed as

$$\underline{H}^{S/C} = I\ \underline{\omega} + \Sigma C_i^T\ \underline{h}_i \tag{7}$$

where C_i is the direction cosine matrix of each gimbal frame $\{\hat{G}\}$ with respect to vehicle frame $\{\hat{\underline{v}}\}$,i.e. $\{\hat{\underline{G}}_i\} = C_i\{\hat{\underline{v}}\}$.

The time derivatives of the total angular momentum of the system with respect to inertial frame $\{\hat{\underline{n}}\}$ is equal to the external torque $\underline{L}_C$ exerted on the system about the mass center c:

$$\underline{L}_C = \frac{d}{dt}\ (\underline{H}^{S/C})_N \tag{8}$$

The above equation can be rewritten as

$$\underline{L}_C = I\dot{\underline{\omega}} + \tilde{\omega} I\underline{\omega} + \Sigma\{\tilde{\omega}\, C_i^T \underline{h}_i + C_i^T\, \dot{\tilde{\sigma}}_i \underline{h}_i\} + \Sigma\, C_i^T\, \dot{\underline{h}}_i$$

where $\tilde{\omega} = \begin{bmatrix} 0 & -\omega_z & \omega_y \\ \omega_z & 0 & -\omega_x \\ -\omega_y & \omega_x & 0 \end{bmatrix}$ and $\dot{\tilde{\sigma}}_i = \begin{bmatrix} 0 & -\dot{\sigma}_i & 0 \\ \dot{\sigma}_i & 0 & 0 \\ 0 & 0 & 0 \end{bmatrix}$.

In the absence of external torques and when the spin rate of wheel is constant, $\underline{L}_C = 0$ and $\dot{\underline{h}}_i = 0$. Thus the system equations of motion are

$$\dot{\underline{\omega}} = -I^{-1}\tilde{\omega}\, I\, \underline{\omega} - I^{-1}\, \Sigma\{\tilde{\omega}\, C_i^T \underline{h}_i + C_i^T \dot{\tilde{\sigma}}_i \underline{h}_i\} \tag{9}$$

SYSTEM CONFIGURATION

In this paper, the pyramid configuration for four CMGs is considered as depicted in Fig. 1. With this configuration, the CMG angular momentum in Eq. (7) can be written as

$$\sum_{i=1}^{4} C_i^T \underline{h}_i = h \begin{bmatrix} -C\delta S\sigma_1 - C\sigma_2 + C\delta S\sigma_3 + C\sigma_4 \\ C\sigma_1 - C\delta S\sigma_2 - C\sigma_3 + C\delta S\sigma_4 \\ S\delta S\sigma_1 + S\delta S\sigma_2 + S\delta S\sigma_3 + S\delta S\sigma_4 \end{bmatrix} \tag{10}$$

where h is the magnitude of each CMG's angular momentum and $\Sigma\, C_i^T\, \dot{\tilde{\sigma}}_i \underline{h}_i$ in Eq. (9) can be written as

$$\sum_{i=1}^{4} C_i^T\, \dot{\tilde{\sigma}}_i \underline{h}_i = C\dot{\underline{\sigma}} = \begin{bmatrix} -C\delta C\sigma_1 & S\sigma_2 & C\delta C\sigma_3 & -S\sigma_4 \\ -S\sigma_1 & -C\delta C\sigma_2 & S\delta_3 & C\delta C\sigma_4 \\ S\delta C\sigma_1 & S\delta C\sigma_2 & S\delta C\sigma_3 & S\delta C\sigma_4 \end{bmatrix} \begin{Bmatrix} \dot{\sigma}_1 \\ \dot{\sigma}_2 \\ \dot{\sigma}_3 \\ \dot{\sigma}_4 \end{Bmatrix}$$

We select $\delta = 54.74^0$ in this configuration to minimize the angular momentum requirements as recommended by Meffe [9]. With this configuration, we consider the preferred initial gimbal angles for some known torque profiles.

Determination of Preferred Initial Gimbal Angles

Perhaps the most severe demand on the CMGs is a unidirectional torque. Bauer [6] shows that for the present CMG configuration and pseudo-inverse steering law, if the torque demand is 1 unit about the x-axis, the CMG cluster encounters an internal singularity at a momentum value of 1.15h. This corresponds to an antiparallel situation. The initial gimbal angles are $\underline{\sigma} = [0^0 \ 0^0 \ 0^0 \ 0^0]^T$ and the angles at the singularity are $\underline{\sigma} = [-90^0 \ 0^0 \ 90^0 \ 0^0]^T$. From Eq. (10), it can be observed that the CMG angular momentum distribution at the singularity is $\underline{H} = [2hc\delta \ 0 \ 0]^T$. To utilize the maximum momentum capability, we calculate the desired final angular momentum corresponding to saturation. At saturation, all the momentum vectors should point along the x-axis, i.e. $\underline{\sigma} = [-90^0 \ 180^0 \ 90^0 \ 0^0]^T$ and $\underline{H} = [h(2c\delta + 2) \ 0 \ 0]^T = [3.1545 \ h \ 0 \ 0]^T$.

With the desired final gimbal angles (perturbed slightly) and a torque demand of $[-1 \ 0 \ 0]^T$, we integrate Eq. (4) backward until the zero angular momentum stage is reached. The preferred set of gimbal angles is obtained as $\underline{\sigma} = [-60^0 \ 60^0 \ 120^0 \ -120^0]^T$. Similarly, several initial gimbal angles are obtained for other desired torques as shown in Table 1. It should be noted that the set $[-120^0 \ -60^0 \ 60^0 \ 120^0]$ is also good for a torque demand of $[1 \ 0 \ 0]^T$. During our experimentation, we found this gimbal angle set could avoid singularities for torques constrained to the x, y directions. However, we did not experiment with time varying torques.

TABLE 1. Preferred Initial Gimbal Angles

Torque Demand	Initial Gimbal Angles
[1 0 0]	[-60° 60° 120° -120°]
[0 1 0]	[-120° -60° 60° 120°]
[0 0 1]	[0° 0° 0° 0°]
[1 1 1]	[0° 0° 0° 0°]
[4 2 0]	[-60° 60° 120° -120°]
[2 4 0]	[-120° -60° 60° 120°]

FEEDBACK CONTROL

Feedback control laws can be determined using the Liapunov stability theory. Vadali and Junkins [10] developed the feedback control laws for spacecraft maneuvers with external torques and reaction wheels. In this section we derive a feedback control law for a slewing maneuver of a spacecraft with CMGs when no external torques exist.

The general equations for attitude and dynamics of the system are given by Equations (6) and (9). Let the target orientation $\underline{\beta}_f^T = [1 \quad 0 \quad 0 \quad 0]$ and the final target angular velocity of vehicle $\underline{\omega}_f^T = [0 \quad 0 \quad 0]$. The error vectors $\underline{e}_1$, and $\underline{e}_2$ which represent the departure of the instantaneous states from the desired terminal states can be written as

$$\underline{e}_1 = \underline{\beta} - \underline{\beta}_f$$

$$\underline{e}_2 = \underline{\omega} - \underline{\omega}_f = \underline{\omega}$$

Let V(e) be a trial Liapunov function defined as

$$V(e) = k\ \underline{e}_1^T\ \underline{e}_1 + \frac{1}{2}\ \underline{e}_2^T\ I\ \underline{e}_2$$

where k is a positive constant. The time derivative of V is given by

$$\dot{V}(e) = 2k\ \underline{e}_1^T\ \dot{\underline{e}}_1 + \underline{e}_2^T I\ \dot{\underline{e}}_2$$

$$= 2k(\underline{\beta}^T - \underline{\beta}_f^T)\ \dot{\underline{\beta}} + \underline{\omega}^T I\dot{\underline{\omega}}$$

Using the identities

$$\underline{\beta}^T\dot{\underline{\beta}} = 0 \quad ,$$

$$\dot{\underline{\beta}} = \frac{1}{2}\ G(\beta)\bar{\omega} \ , \text{ and}$$

$$I\dot{\underline{\omega}} = -\tilde{\omega}\ I\underline{\omega} - \Sigma(\tilde{\omega}\ C_i^T\underline{h}_i + C_i^T\ \tilde{\dot{\sigma}}_i\underline{h}_i) \ ,$$

$\dot{V}(\underline{e})$ can be written as

$$\dot{V}(e) = -k\ \underline{\beta}_f^T\ G(\beta)\bar{\omega} + \underline{\omega}^T\{-\tilde{\omega}I\underline{\omega} - \Sigma(\tilde{\omega}C_i^T\underline{h}_i + C_i^T\ \tilde{\dot{\sigma}}_i\underline{h}_i)\}$$

However, $\underline{\omega}^T\tilde{\omega} = 0$ and $-k\beta_f^T G(\underline{\beta})\bar{\omega} = -\underline{\omega}^T(-k\bar{\beta})$
where $\bar{\beta}^T = [\beta_1\ \beta_2\ \beta_3]$. Hence $\dot{V}(\underline{e})$ can be simplified as

$$\dot{V}(e) = -\underline{\omega}^T(-k\bar{\beta} + \Sigma C_i^T\ \tilde{\dot{\sigma}}_i\underline{h}_i).$$

For $\dot{V}(e)$ to be negative definite, we can choose a linear feedback control as

$$-k\bar{\beta} + \Sigma\, C_i^T\, \tilde{\dot{\sigma}}_i \underline{h}_i = K\underline{\omega}$$

where K is a positive definite constant matrix

$$K = \begin{bmatrix} K_1 & 0 & 0 \\ 0 & K_2 & 0 \\ 0 & 0 & K_3 \end{bmatrix} .$$

$\Sigma\, C_i^T\, \tilde{\dot{\sigma}}_i \underline{h}_i$ can be written as $C\underline{\dot{\sigma}}$ where C is a matrix whose rows compose of first row of directoin cosine matric C_i of each CMG gimbal frame with respect to $\{\hat{\underline{V}}\}$. Then the feedback control law becomes

$$C\underline{\dot{\sigma}} = K\underline{\omega} + k\bar{\beta}.$$

Usually the number of CMGs cluster is more than three. Then we can choose the minimum norm solution for a rate control $\underline{\dot{\sigma}}$ as

$$\underline{\dot{\sigma}} = C^+ (K\underline{\omega} + k\bar{\beta}) \qquad (11)$$

where C^+ is a pseudo-inverse of C.

Thus we have the same form for $\underline{\dot{\sigma}}$ as Eq. (4).

Simulation

Equations (6), (9) and (11) are a complete set of equations which are needed for a simulation. With a pyramid configured CMG cluster as depicted in

Fig. 1, we present a simulation of a slewing maneuver. For critical damping, the gains K and k are chosen as [10]

$$K_i^2 = 2I_i k \qquad (i = 1,2,3)$$

The numerical data and boundary conditions are shown in Table 2 and Table 3. Near a singularity, the determinant of CC^T becomes almost zero. The required magnitude of control rate $|\dot{\sigma}_i|$ increases enormously and exceeds the control limit $|\dot{\sigma}|_{limit}$. To avoid a singularity, Cornick [4] suggests a method using the "null" motion. However, in this paper we choose the determinant test to avoid a singularity. That is, when det. (CC^T) is less than $Det._{limit}$, we simply hold $\dot{\sigma}$ at its most previous value. After escaping from a singularity, we use the pseudo-inverse technique again. The selection of $Det._{limit}$ is based on the required $|\dot{\sigma}_{limit}|$.

The simulation results show that without any method of avoiding singularity, the determinant of CC^T becomes almost zero many times as depicted in Fig. 3. When using the determinant test method, many would-be singular points are passed through with reasonable gyro rates although during the passages there are some fluctuations in gyro rates as depicted in Fig. 4 and Fig. 5. However, the feedback control law works very well as shown in Figs. 6 and 7. The gimbal angles are shown in Fig. 8 and the demanded torques in Fig. 9. The maneuver takes about 170 sec.

TABLE 2. Numerical Data

Item	Values
I_x	86.215 kg-m^2
I_y	85.07 kg-m^2
I_z	113.565 kg-m^2
h	1.8 kg-m^2
k_1	13.13 N-m-sec
k_2	13.04 N-m-sec
k_3	15.08 N-m-sec
k	1.0 N-m
δ	54.74°
Det_{limit}	0.1

TABLE 3. Boundary Conditions

State	Initial Conditions	Final Conditions
β_0	0.7071	1
β_1	0.7071	0
β_2	0	0
β_3	0	0
ω_x	0.01 r/sec	0
ω_y	0.05 r/sec	0
ω_z	0.001 r/sec	0

CONCLUSION

Rotational maneuvers of spacecraft with single-gimbal CMGs is treated. The fact that some sets of initial gimbal angles avoid singularities for unidirectional and planar torque demands is observed. The feedback control law based on Liapunov theory works well with the single-gimbal CMG system. Avoidance of large fluctuations in $\dot{\underline{o}}$ needs further study.

REFERENCES

[1] Margulies, G and Aubrun, J.N., "Geometric Theory of Single-Gimbal Control Moment Gyro Systems," J. of Astronautical Sciences, Vol. XXVI, No. 2, pp. 159-191, April-June 1978.

[2] Kennel, H.F., "Steering Law for Parallel Mounted Double-Gimballed Control Moment Gyros - Revision A," NASA TM-82390, Jan. 1981.

[3] Yoshikawa, T., "Steering Law for Roof Type Configuration Control Moment Gyro System," Automatica, Vol. 12, pp. 359-368, 1977.

[4] Cornick, D.E., "Singularity Avoidance Control Laws for Single Gimbal Control Moment Gyros," AIAA paper No. 79-1698, Aug. 1979.

[5] Hefner, R.D. and McKenzie, C.H., "A Technique for Maximizing the Torque Capability of Control Moment Gyro Systems," AAS paper No. 83-387.

[6] Bauer, S.R., "Single Gimbal CMG Steering Laws," SGNM No. 10E-87-06, 10E-87-09, Charles Stark Draper Laboratory, Inc., May 1987.

[7] Junkins, J.L. and Turner, J.D., Optimal Spacecraft Rotational Maneuvers, studies in Astronautics 3, Elsevier Scientific Publishing Company, New York, 1985.

[8] Ross, I.M. and Melton, R.G., "Quaternion Formulation of Rotational Dynamics for a Double-Gimbaled Momentum Wheel Control System," AAS paper No. 87-510, August 1987.

[9] Meffe, M., "Control Moment Gyroscope Configurations for the Space Station," AAS paper No. 88-040, Jan.-Feb. 1988.

[10] Vadali, S.R. and Junkins, J.L., "Optimal Open-Loop and Stable Feedback Control of Rigid Spacecraft Attitude Maneuvers," J. of the Astronautical Sciences, Vol. 32, No. 2, April-June 1984, pp. 105-122.

NOMENCLATURE

$\underline{H}^{s/c}$: angular momentum of system about mass center c in vehicle frame $\{\hat{\underline{v}}\}$

$\underline{H}^{v/c}$: angular momentum of vehicle about mass center c in $\{\hat{\underline{v}}\}$

$\underline{H}^{G_i/c}$: angular momentum of gyro about mass center c in $\{\hat{\underline{v}}\}$

$\underline{H}^{G_i/cG_i}$: angular momentum of gyro about gyro mass center cG_i in $\{\hat{\underline{v}}\}$

$I^{v/c}$: inertia matrix of vehicle about c with respect to vehicle frame $\{\hat{\underline{v}}\}$

I : inertia matrix of vehicle and point-massed gyro clusters about c with respect to $\{\hat{\underline{v}}\}$

M_i : i^{th} gyro point-massed inertia matrix about c with respect to $\{\hat{\underline{v}}\}$.

$\underline{h}_i$: i^{th} gyro relative angular momentum in gimbal frame, $\underline{h}_i^T = [0\ h\ 0]$

m_i : i^{th} gyro mass

$c\delta$: $\cos(\delta)$

$s\delta$: $\sin(\delta)$

δ : configuration angle of pyramid

$\underline{\omega}$: spacecraft angular velocity, $\underline{\omega}^T = [\omega_x\ \omega_y\ \omega_z]$

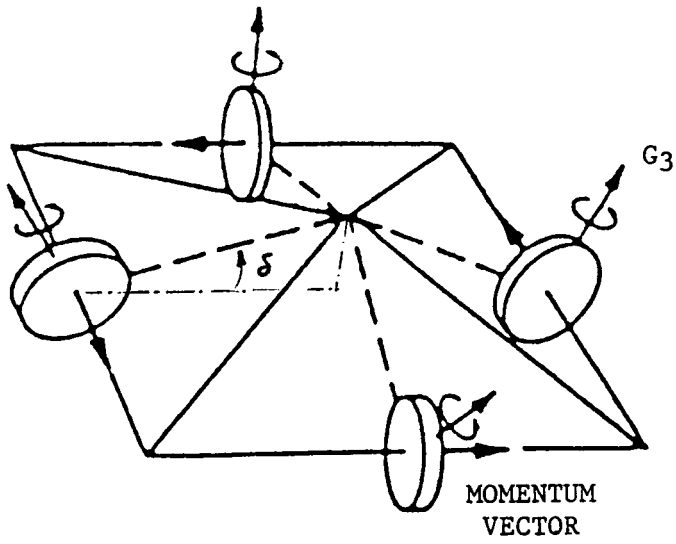

Fig. 1. CMG Configuration

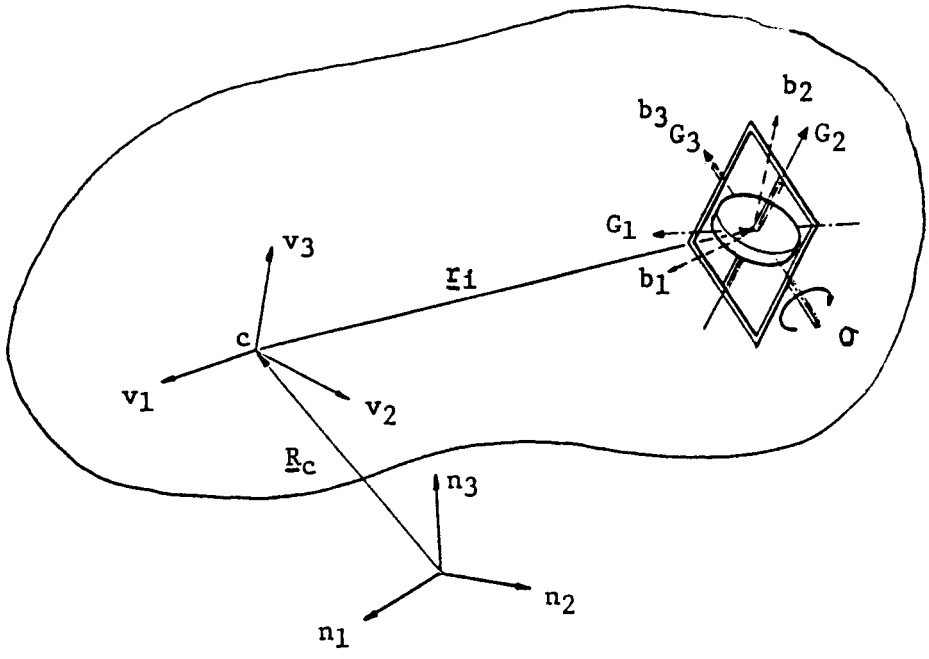

Fig. 2. System with i^{th} gyro

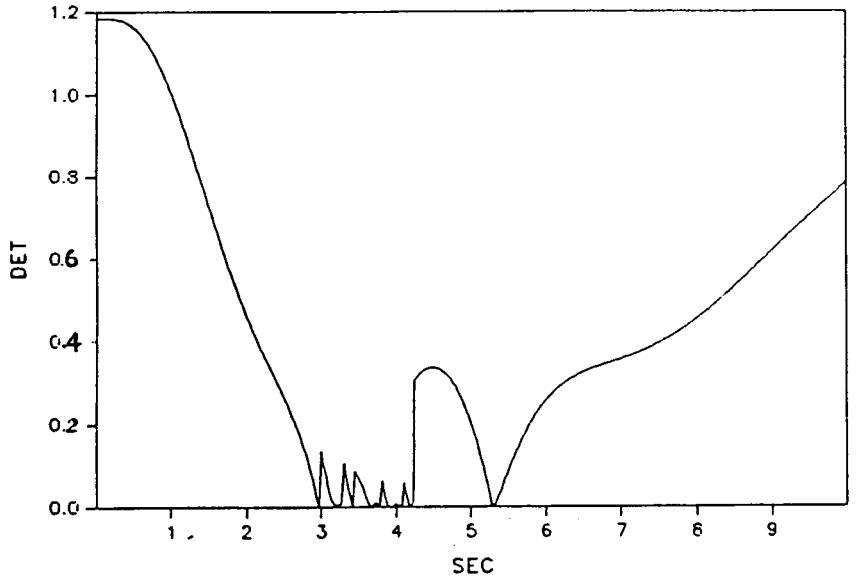

Fig. 3. Determinant of (CC^T) w/o bounds on control

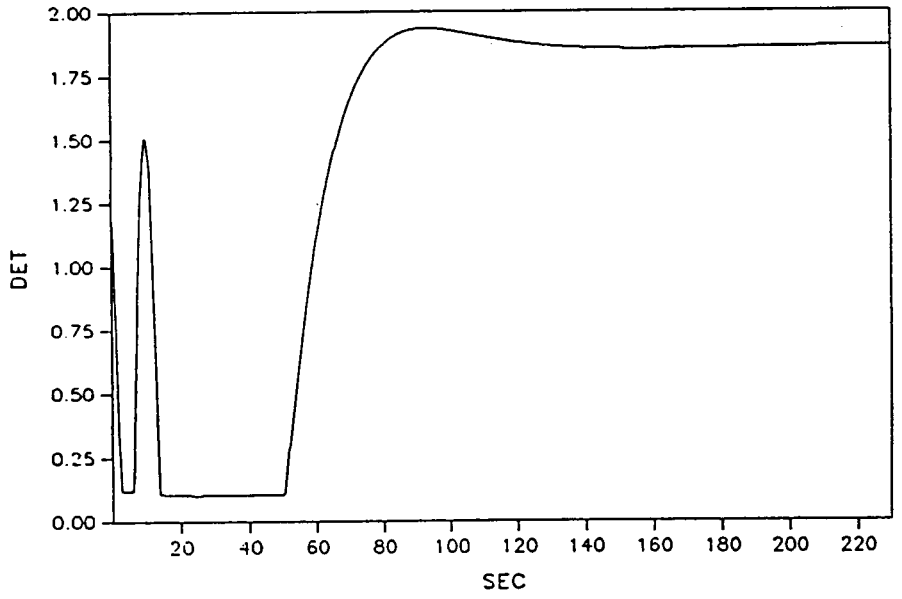

Fig. 4. Determinant of (CC^T) with limit $Det._{lim.}$

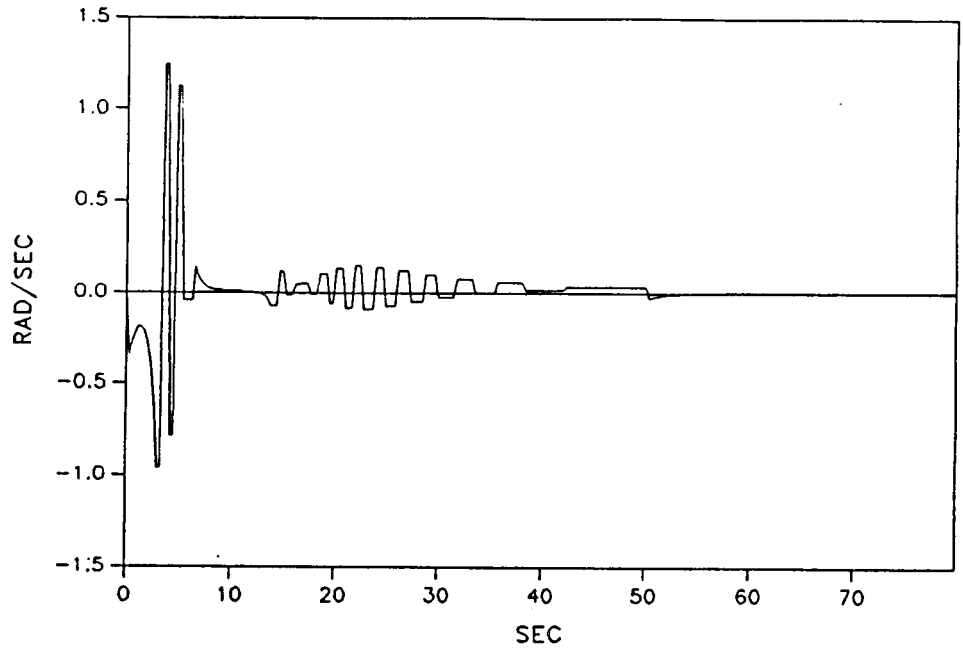

(a) The 1st gyro gimbal rate

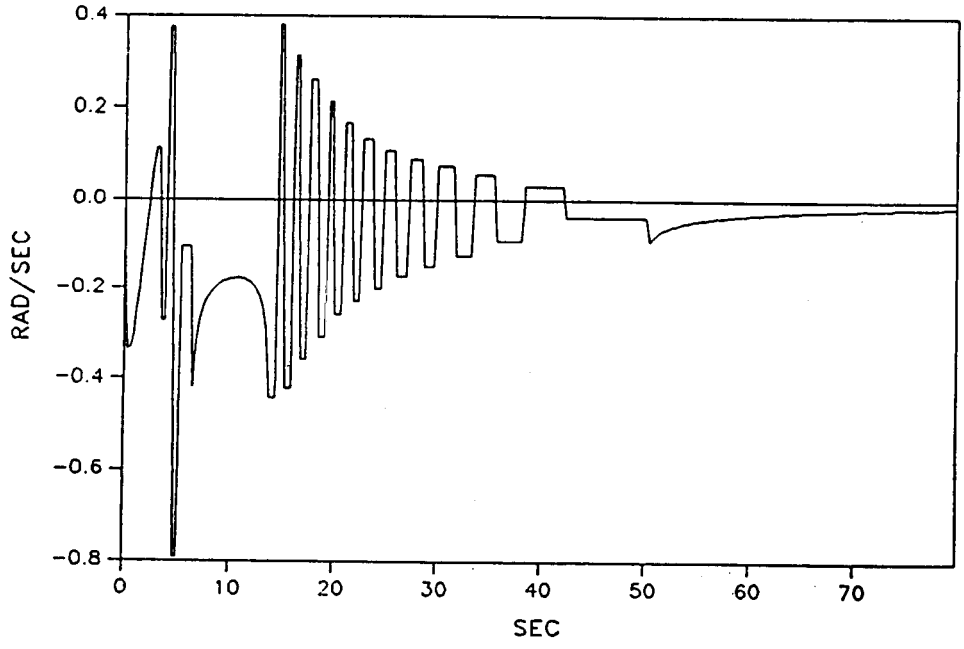

(b) The 2nd gyro gimbal rate

Fig. 5 Gyro gimbal rates

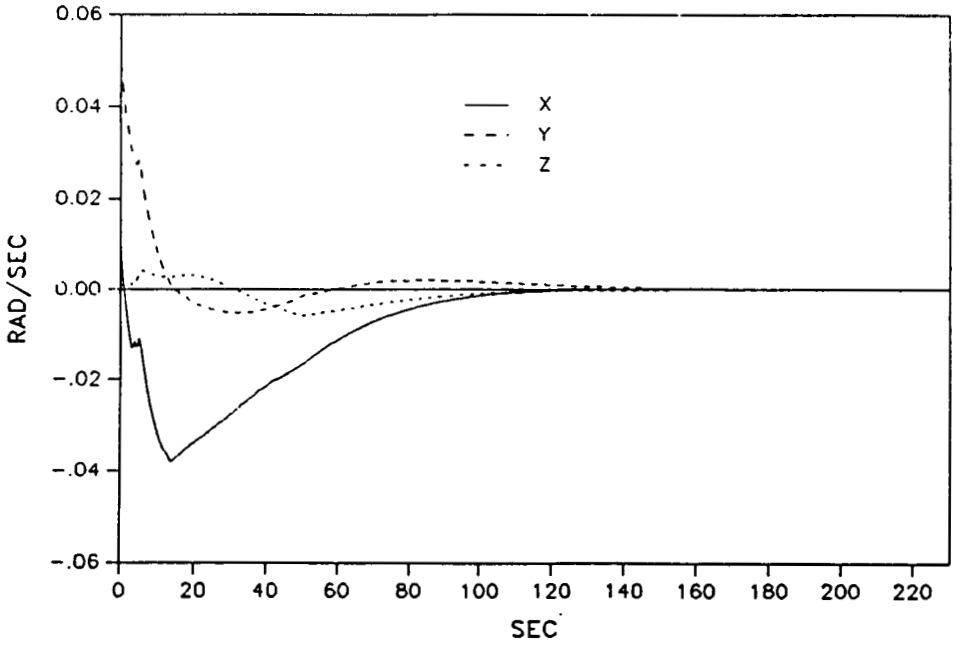

Fig. 6. Angular velocities of spacecraft

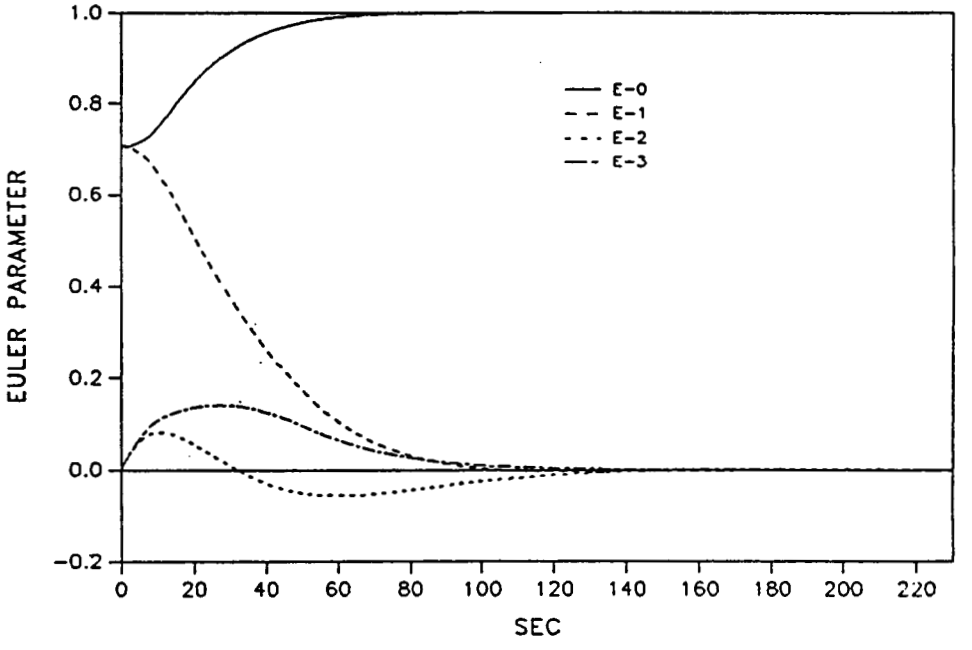

Fig. 7. Attitude of spacecraft

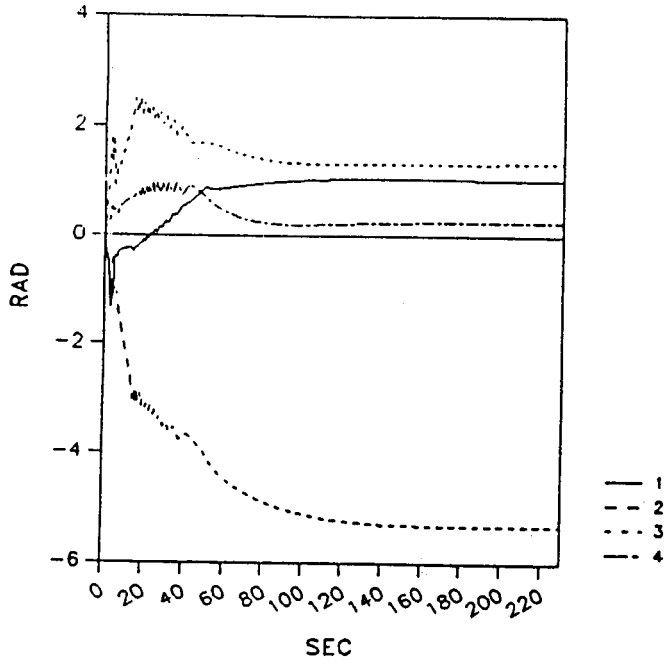

Fig. 8. Gimbal angles

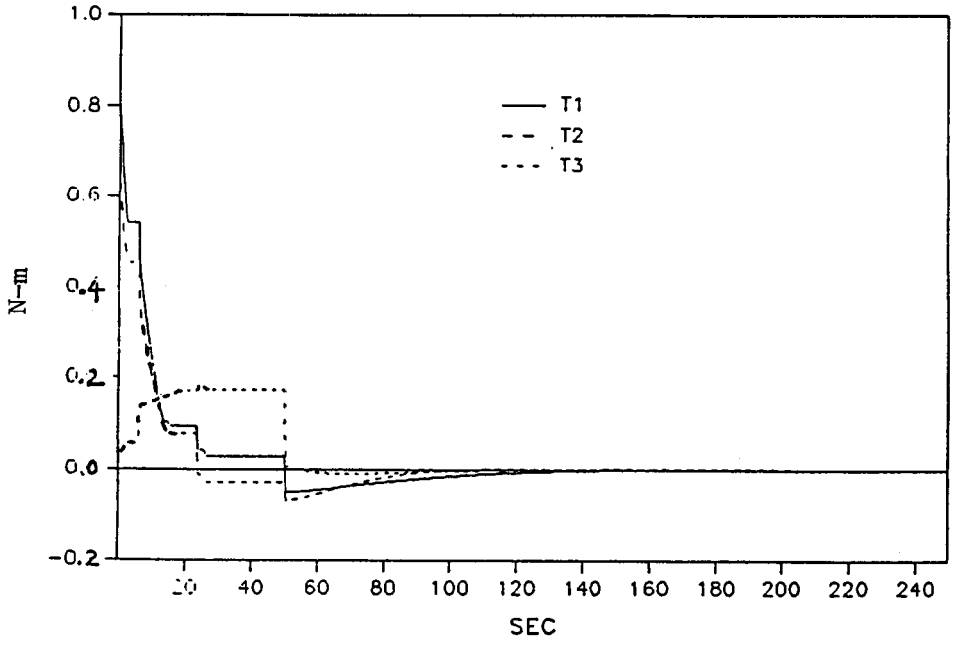

Fig. 9. Torque demands